Nat. Hazards Earth Syst. Sci. Discuss., 1, 5087–5115, 2013
www.nat-hazards-earth-syst-sci-discuss.net/1/5087/2013/
doi:10.5194/nhessd-1-5087-2013

Natural Hazards and Earth System Sciences
Open Access
Discussions

Numerical investigation of stability of breather-type solutions of the nonlinear Schrödinger equation

A. Calini[1] **and C. M. Schober**[2]

[1]Department of Mathematics, College of Charleston, Charleston SC 29424, USA
[2]Department of Mathematics, University of Central Florida, Orlando, FL, USA

Received: 1 September 2013 – Accepted: 9 September 2013 – Published: 27 September 2013

Correspondence to: C. M. Schober (cschober@ucf.edu)

Published by Copernicus Publications on behalf of the European Geosciences Union.

Abstract

In this article we present the results of a broad numerical investigation on the stability of breather-type solutions of the nonlinear Schrödinger (NLS) equation, specifically the one- and two-mode breathers for an unstable plane wave, which are frequently used to model rogue waves. The numerical experiments involve large ensembles of perturbed initial data for six typical random perturbations. Ensemble estimates of the "closeness", $\mathcal{A}(t)$, of the perturbed solution to an element of the respective unperturbed family indicate that the only neutrally stable breathers are the ones of maximal dimension, that is: given an unstable background with N unstable modes, the only neutrally stable breathers are the N-dimensional ones (obtained as a superimposition of N simple breathers via iterated Backlund transformations). Conversely, breathers which are not fully saturated are sensitive to noisy environments and are unstable. Interestingly, $\mathcal{A}(t)$ is smallest for the coalesced two-mode breather indicating the coalesced case may be the most robust two-mode breather in a laboratory setting. The numerical simulations confirm and provide a realistic realization of the stability behavior established analytically by the authors.

1 Introduction

Interest in understanding rogue wave phenomena has been steadily growing for the past decade, especially with current concerns over potential climate changes and their affect on the likelihood and height of rogue waves. The focusing nonlinear Schrödinger (NLS) equation

$$iu_t + u_{xx} + 2|u|^2 u = 0, \tag{1}$$

often appears in studies of rogue wave formation in deep water when wave amplification is assumed to be primarily due to nonlinear focusing and the modulational instability. As a result, several classes of solutions of the NLS equation are considered

NHESSD
1, 5087–5115, 2013

to be prototypes of rogue waves. For periodic boundary conditions, $u(x+L,t) = u(x,t)$, one such family is the family of homoclinic orbits of unstable plane waves with N unstable modes (Dysthe and Trulsen, 1999; Osborne et al., 2000; Calini and Schober, 2002; Akhmediev et al., 2009a). We will refer to these homoclinic orbits, which can have $M \leq N$ modes excited, as M-mode spatially periodic breather (SPB) solutions (see Figs. 1 and 2). Time- periodic breather-type solutions as well as rational solutions which arise as singular limits of breather-type solutions and which decay polynomially in space and time have also been studied (Ankiewicz et al., 2010; Akhmediev et al., 2009b; Ohta and Yang, 2012).

For modeling purposes, the issue of robustness of these families of solutions is important. To successfully observe or reproduce rogue waves in a setting where noise and small higher order nonlinear effects are inherent requires: (i) solutions to remain close when there are small random variations initially and (ii) persistence in perturbations of the NLS equation. In this article we take a closer look at the stability of the one-mode SPBs over a plane wave with one or two unstable modes (UMs) and the two-mode SPBs over a plane wave with two UMs. In Sect. 2 we recall the basic elements of the associated Floquet theory which allows for an exploration of the structure and properties of the SPB solutions. Section 3, the focus of this paper, provides the results of a broad numerical investigation of the stability of the SPBs with respect to a wide range of initial perturbations $f_i(x)$. We consider (i) random shifts in the initial phase (ii) random spatial perturbations in the height of the wave, (iii) random noise, (iv) localized random gaussian perturbations, and (v and vi) random high and low frequency perturbations. For each type of SPB and for each $f_i(x)$ an ensemble of 100 numerical experiments was carried out varying the random component in the initial data.

To study reproducibility/stability numerically, we first find the "closest" element of the family of SPBs to the perturbed solution. Varying the parameters of the family and using the H_1-norm to measure distances, the closest element is found my minimizing the maximum distance between the perturbed solution and the members of the family of SPBs. Contour plots provide another diagnostic since they are visually intuitive and

NHESSD
1, 5087–5115, 2013

show when solutions stay structurally close to each other in "shape". The ensemble estimates of closeness, $\mathcal{A}(t)$, indicate that the only neutrally stable SPBs are those for which all the instabilities of the underlying plane wave are saturated, e.g. the two-mode SPB over a plane wave with two UMs. In the numerical simulations the perturbed SPBs may develop a small spatial asymmetry due to the random perturbations. Interestingly, when considering the family of two-mode SPBs, $\mathcal{A}(t)$ is smallest for the coalesced two-mode SPB since the spatial asymmetry is minimized. The authors studied the persistence of one- and two-mode SPBs for several perturbed NLS models on a periodic domain (Calini and Schober, 2002, 2009); numerical simulations and Melnikov arguments indicated the persistence under perturbation of the coalesced two-mode SPB. These two observations indicate the coalesced case may be the most robust two-mode SPB in a laboratory setting. Conversely, SPBs which are not fully saturated are sensitive to noisy environments and are unstable. Finally, in Sect. 4 we outline our linear stability analysis of the one- and two-mode SPBs which support the results of the numerical investigation.

2 Analytical background

In this section we provide the necessary elements of the associated Floquet spectral theory to enable a study of the stability of the SPBs. The NLS equation is equivalent to the consistency of the following Zakharov–Shabat linear system (Z–S) (Zakharov and Shabat, 1972)

$$\mathcal{L}^{(x)}\mathbf{v} = \begin{pmatrix} \frac{\partial}{\partial x} + i\lambda & -u \\ u^* & \frac{\partial}{\partial x} - i\lambda \end{pmatrix} \mathbf{v} = 0$$

$$\mathcal{L}^{(t)}\mathbf{v} = \begin{pmatrix} \frac{\partial}{\partial t} - i(|u|^2 - 2\lambda^2) & -iu_x - 2\lambda u \\ -iu_x^* + 2\lambda u^* & \frac{\partial}{\partial t} + i(|u|^2 - 2\lambda^2) \end{pmatrix} \mathbf{v} = 0, \quad (2)$$

NHESSD
1, 5087–5115, 2013

where λ is the spectral parameter and $u(x,t)$ is a solution of the NLS equation itself.

The spectrum of $\mathcal{L}^{(x)}$ is defined by

$$\sigma(\mathcal{L}^{(x)}) := \{\lambda \in \mathbb{C} | \mathcal{L}^{(x)}\mathbf{v} = 0, |\mathbf{v}| \text{ bounded } \forall x\}, \tag{3}$$

and for $u(x+L,t) = u(x,t)$ the spectrum is obtained using Floquet theory. Starting with the monodromy matrix of Eq. (2), $M(x;u,\lambda)$, and letting $\Delta(u,\lambda) := \mathrm{tr}M(L;u,\lambda)$, the spectrum is given by the following condition on the discriminant $\Delta(u,\lambda)$:

$$\sigma(\mathcal{L}^{(x)}) := \{\lambda \in \mathbb{C} | \Delta(u,\lambda) \in \mathbb{R}, -2 \leq \Delta(u,\lambda) \leq 2\}. \tag{4}$$

Of particular interest are the following elements of the periodic spectrum:

1. The simple spectrum, $\sigma^{\mathrm{s}} = \{\lambda_j^{\mathrm{s}} | \Delta(u,\lambda) = \pm 2, d\Delta/d\lambda \neq 0\}$.
2. Double points of the spectrum, $\sigma^{\mathrm{d}} = \{\lambda_j^{\mathrm{d}} | \Delta(u,\lambda) = \pm 2, d\Delta/d\lambda = 0, d^2\Delta/d\lambda^2 \neq 0\}$.

The spectrum of $\mathcal{L}^{(x)}$ is invariant under the NLS flow and each periodic eigenvalue determines the structure and dynamical stability of the corresponding nonlinear mode. In particular there are no instabilities associated with λ_j^{s} or real λ_j^{d}, whereas linear instabilities arise when the λ_j^{d} are complex.

To illustrate the relation between the number of complex λ_j^{d} and the number of instabilities, we consider the plane wave solution $u_a(t) = ae^{\mathrm{i}(2a^2t+\phi)}$. For small perturbations $u(x,t) = u_a(t)(1+\epsilon(x,t))$, $|\epsilon| \ll 1$, ϵ satisfies

$$i\epsilon_t + \epsilon_{xx} + 2|a|^2(\epsilon + \epsilon^*) = 0. \tag{5}$$

Thus $\epsilon \propto e^{i\mu_j x + \sigma_j t}$ where $\mu_j = 2\pi j/L$ and $\sigma_j^2 = \mu_j^2(4|a|^2 - \mu_j^2)$. The solution is unstable if $0 < (j\pi/L)^2 < |a|^2$ and the number of unstable modes (UMs) is the largest integer M such that $0 < M < |a|L/\pi$. On the other hand, the discriminant of the plane wave

NHESSD
1, 5087–5115, 2013

is $\Delta(a;\lambda) = 2\cos(\sqrt{a^2+\lambda^2}L)$. The discrete spectrum is given by $\lambda_0^{\mathrm{s}} = \pm ia$ and $(\lambda_j^{\mathrm{d}})^2 = (\frac{j\pi}{L})^2 - a^2$, $j \neq 0$. Notice that the λ_j^{d} are complex if $0 < (j\pi/L)^2 < |a|^2$ which is the same condition for a mode to be linearly unstable.

2.1 SPBs over an unstable plane wave

Explicit representations for the SPBs can be constructed using the Bäcklund-gauge transformation for the NLS equation (see Sect. 4). For an unstable plane wave with N UMs, a single Bäcklund transformation at a complex λ_j^{d} generates the one-mode SPB family corresponding to the jth unstable mode,

$$\begin{aligned} U^{(j)}(x,t;\rho) = & a e^{\mathrm{i}(2a^2 t+\phi)} \\ & \times \left[\cos 2p_j - \sin p_j \,\mathrm{sech}(\rho-\sigma_j t)\cos(2\pi j x/L+\beta)\right. \\ & \left. +\mathrm{i}\sin 2p_j \tanh(\rho-\sigma_j t)\right] \\ & \times \left[1+\sin p_j \,\mathrm{sech}(\rho-\sigma_j t)\cos(2\pi j x/L+\beta)\right]^{-1}, \end{aligned} \tag{6}$$

The parameter ρ governs the time at which the mode becomes excited, β_j is related to spatial shifts in the solution, $\mu_j = 2\pi j/L$, and $p_j = \arccos \pi j/aL$. The one-mode SPB limits to a phase translation of the plane wave as $t \to \pm\infty$ with the decay rate σ_j. For example, Fig. 1a and b show the amplitudes of the two different one-mode SPBs, $U^{(1)}(x,t;\rho)$ and $U^{(2)}(x,t;\rho)$, over an unstable plane wave with two UMs for $a = 0.5$, $L = 4\sqrt{2}\pi$, $\rho = \phi = \beta = 0$, and $x \in [-L/2, L/2]$, $t \in [-10, 10]$. The one-mode SPB over an unstable plane wave with one UM has the same structure as in Fig. 1a, L is simply adjusted to allow for only one UM. In the next sections we show that the one-mode SPB is neutrally stable and reproducible only when the underlying plane wave has one UM.

To find a higher dimensional M-mode SBP ($1 < M \leq N$) requires M iterations of the the Bäcklund-gauge transformation (see Eq. 17) since at each step we also need to

NHESSD
1, 5087–5115, 2013

know the corresponding eigenfunctions of the Lax pair. Each iteration of the transformation introduces an additional parameter in the resulting solution. Applying the Bäcklund-gauge transformation successively at complex λ_1^d and λ_2^d generates a two-mode SPB family of the form (see Calini and Schober, 2002 for the exact formula):

$$U^{(1,2)}(x,t;\rho,\tau) = a e^{2ia^2 t}\,\frac{N(x,t;\rho,\tau)}{D(x,t;\rho,\tau)}. \tag{7}$$

The amplitude of Eq. (7) is shown in Fig. 2a where the two spatial modes are distinct with $\rho = -2$, $\tau = -5$, $a = 0.5$, $L = 4\sqrt{2}\pi$, $t \in [-10, 10]$. Figure 2a shows the two-mode SPB can be thought of as a nonlinear superposition of two one-mode SPBs with spatial modes $\cos(\mu_1 x + \beta_1)$ and $\cos(\mu_2 x + \beta_2)$. As before, as $t \to \pm\infty$ the 2-mode SPB approaches a phase translation of the plane wave exponentially fast.

The parameters ρ and τ determine the time at which the first and second mode, respectively, become excited. Ultimately ρ and τ govern the shape, amplitude, and steepness of the SPB since they can be adjusted to excite the modes at the same time ($\rho = -2$, $\tau = -3$). We refer to this case as the coalesced two-mode SPB, see Fig. 2b. Surprisingly, as we will see in the next section, even though the coalesced two-mode SPB has steeper gradients, it can be more robust to random perturbations of the inital data than a generic two-mode SPB.

3 Numerical evidence of stability

To integrate the NLS Eq. (1) with periodic boundary conditions we use a highly accurate and efficient exponential integrator that uses Pade rational-function approximations to the exponential, a Fourier-mode decomposition in space and a fourth-order RK discretization in time (Khaliq et al., 2009). This scheme has extensively been tested with a variety of known analytical solutions. For example, using $N = 256$ Fourier modes in space and a timestep $\Delta t = 10^{-3}$, we find that the H^1-norm of the difference between

NHESSD
1, 5087–5115, 2013

the analytical and numerical solutions is at most $\mathcal{O}(10^{-12})$. On the other hand, the error in the global invariants, the norm, the momentum and the Hamiltonian is at most $\mathcal{O}(10^{-9})$.

For simplicity we examine the stability of the one- and two-mode SPB solutions. The results are generalizable to the case of an M mode breather over an unstable plane wave with $N \geq M$ unstable modes (UMs). We start by letting

$$U_\epsilon(x,0) = U^{(j)}(x,0;\rho) + \epsilon f_i(x), \quad j = 1,2 \tag{8}$$

or

$$U_\epsilon(x,0) = U^{(1,2)}(x,0;\rho,\tau) + \epsilon f_i(x), \tag{9}$$

where ϵ should be on the order of experimental error, $0 < \epsilon \ll 1$. The parameters ρ and τ are selected so that $U^{(j)}(x,0;\rho)$ or $U^{(1,2)}(x,0;\rho,\tau)$ are not too close to the unstable plane wave in order to avoid exciting any of its instabilities. In all the numerical experiments the perturbation parameter $\epsilon = 10^{-4}$ and the time frame is $t \in [0,30]$. There is an inherent limitation to the time frame considered since for longer times the solutions will enter a neighborhood of the plane wave.

Three cases are under consideration: $U^{(j)}(x,t)$ over the plane wave with (i) $N = 1$ or (ii) $N = 2$ UMs and (iii) $U^{(1,2)}(x,t)$ over the plane wave with $N = 2$ UMs. If $U_\epsilon(x,t)$ remains close, in an appropriate sense to be discussed below, to an element of the respective family, $U^{(j)}(x,t;\rho))$ or $U^{(1,2)}(x,t;\rho,\tau)$, then this indicates the SPB is neutrally stable; otherwise it is unstable.

In each of the three cases (i–iii) and for each of the following perturbations $f_i(x), i = 1,\ldots,6$, shown in Fig. 3, an ensemble of 100 numerical experiments was carried out by varying the random component in the intial data:

a. $f_1(x) = \cos 2\pi k(x+\phi)/L$, $k = 1,2$ where $\phi \in [0,1]$ is a random shift in the phase;

b. $f_2(x) = r(x)\cos 2\pi kx/L$,$k = 1,2$, where $r(x) \in [0,1]$ is a spatially random perturbation in the height of the wave;

NHESSD
1, 5087–5115, 2013

c. $f_3(x) = r(x)$ where $r(x) \in [0,1]$ is random noise;

d. $f_4(x) = \sum_{k=1}^{J} r_k(x) e^{-(x-x_j)^2}$, where $r_j(x) \in [0,1]$ are random fields. This represents a set of localized gaussian perturbations about the points x_j;

e. $f_5(x) = \sum_{k=-K}^{K} r_k(x) e^{i2\pi kx/L}$ for small K, where $r_k(x) \in [0,1]$ are random fields. This gives a low frequency perturbation;

f. $f_6(x) = \left(\sum_{k=-K}^{-K+2} + \sum_{k=K-2}^{K}\right) r_k(x) e^{i2\pi kx/L}$ for large K, where $r_k(x) \in [0,1]$ are random fields. This gives a high frequency perturbation.

To study reproducibility/stability, in the numerical experiments we examine the evolution of the norm of the difference of the perturbed solution with the closest element of the unperturbed family. For example, in the case of a one-mode SPB, i.e. solution Eq. (6), we start with

$$\mathcal{H}^{(j)}(t;\rho) = \|U_\epsilon(x,t) - U^{(j)}(x,t;\rho)\|_{H^1}. \tag{10}$$

To determine the closest element of $U^{(j)}(x,t;\rho)$ to the perturbed solution we let

$$\mathcal{H}^{(j)}_{\max}(\rho) = \max_{t\in[0,30]} \mathcal{H}^{(j)}(t;\rho) \tag{11}$$

and then determine the parameter value ρ^* which minimizes $\mathcal{H}^{(j)}_{\max}(\rho)$, i.e

$$\mathcal{H}^{(j)}_{\mathrm{mm}} = \min_\rho \mathcal{H}^{(j)}_{\max}(\rho) = \mathcal{H}^{(j)}_{\max}(\rho^*). \tag{12}$$

As such, $U^{(j)}(x,t;\rho^*)$ is the closest element and the evolution of $\mathcal{H}^{(j)}(t;\rho^*)$ provides a measurement of how close the perturbed solution is to an element of the one-mode SPBs. We estimate an ensemble measure of "closeness" using $\mathcal{A}^{(j)}_i(t)$, the average of $\mathcal{H}^{(j)}(t;\rho^*)$ over all 100 simulations, for each f_i (note that ρ^* is different for each simulation).

NHESSD
1, 5087–5115, 2013

We also use contour plots as a reproducibility/stability diagnostic since they are visually intuitive and show when solutions stay structurally close to each other in "shape", a feature which can't be determined by examination of $\mathcal{A}_i^{(j)}(t)$ alone. In the contour plots we superimpose the contour of the amplitude obtained from the numerically generated solution $U_\epsilon(x,t)$ on that of the respective unperturbed analytical solution, $U^{(j)}(x,t;\rho^*)$ or $U^{(1,2)}(x,t;\rho^*,\tau)$. Although we present only sample contour plots for the different cases, the graphs of $\mathcal{A}_i^{(j)}(t)$ provide the information obtained from the entire ensemble for each perturbation f_i. The numerical results consistently indicate that only the SPBs with all the instabilities of the underlying plane wave staturated are neutrally stable.

Case one: We consider the one-mode SPB over a plane wave with one UM, Eq. (6) with $j=1$, $a=0.5$ and $L=2\sqrt{2}\pi$. Figure 4a shows $\mathcal{H}_{\max}^{(1)}(\rho)$ for $U_\epsilon(x,0)=U^{(1)}(x,0;\rho)+\epsilon f_3(x)$. Note that $\mathcal{H}_{\mathrm{mm}}^{(1)}\sim$ occurs at $\rho^*\sim 5.04$. The contours of $|U_\epsilon(x,t)|$ and of $|U^{(1)}(x,t;\rho^*)|$, the nearest one-mode SPB found by minimizing $\mathcal{H}_{\max}^{(1)}(\rho)$, are given in Fig. 4b. Here, $U_\epsilon(x,t)$ and the nearest SPB are visually identical. Figure 4c provides the evolution of $\mathcal{A}_i^{(1)}(t)$ for each random $f_i(x)$. The small growth in $\mathcal{A}_i^{(1)}(t)$ to 10^{-3} at $t\approx 11$ for all $f_i(x)$ is due to a small spatial asymmetry which develops in the perturbed solution due to the random nature of the $f_i(x)$. This growth is not significant – compare it to the growth in $\mathcal{A}_i^{(1)}(t)$ or $\mathcal{A}_i^{(2)}(t)$ in Figs. 5 or 6 when the underlying plane wave has two UMs. These results show the perturbed solution stays near to $U^{(1)}(x,t;\rho^*)$ for a substantial period of time, indicating the one-mode SPBs are neutrally stable when the underlying plane wave has only one mode.

Case two: Next we consider the one-mode SPB over a plane wave with two UMs, Eq. (6) with $j=1,2$, $a=0.5$ and $L=4\sqrt{2}\pi$. The contours of $|U_\epsilon(x,t)|$ for $U_\epsilon(x,0)=U^{(1)}(x,0;\rho)+\epsilon f_1(x)$ (where $k=2$ in $f_1(x)$) and of $|U^{(1)}(x,t;\rho^*)|$, are given in Fig. 5a. The closest one-mode SPB found by minimizing $\mathcal{H}_{\max}^{(1)}(\rho)$ matches only the first mode of the perturbed solution. A second mode is excited in the perturbed solution at $t\approx 20$ which does not develop in any element of $|U^{(1)}(x,t;\rho)|$. In Fig. 5b the ensemble mea-

NHESSD
1, 5087–5115, 2013

sure of closeness, $\mathcal{A}_i^{(1)}(t)$, shows rapid large growth to $\mathcal{O}(10)$ when this second mode develops. This second mode is excited in $U_\epsilon(x,t)$ for all random $f_i(x)$ and, in fact the maximum of $\mathcal{A}_i^{(1)}(t)$ is larger for the other perturbations. Figure 6a shows the corresponding contours when $U_\epsilon(x,0) = U^{(2)}(x,0;\rho) + \epsilon f_1(x)$ (for $k = 1$ in $f_1(x)$). Similar rapid growth in $\mathcal{A}_i^{(2)}(t)$ is observed, Fig. 6b, indicating the one-mode SPBs are unstable over plane waves with $N \geq 2$ UMs.

Case three: Finally we consider the two-mode SPB over a plane wave with two UMs, expression (7) with $i = 1$, $j = 2$, $a = 0.5$ and $L = 4\sqrt{2}\pi$. In this case we need to find the element of the family $U^{(1,2)}(x,t;\rho,\tau)$ closest to $U_\epsilon(x,t)$. The parameters ρ and τ determine the time when the first and second modes of the SPB become excited. We successively find ρ^* and then τ^*, which minimize the differences of the first and second developing modes between the perturbed and unpertubed solutions, respectively. Generalizing, let

$$\mathcal{H}^{(1,2)}(t;\rho^*,\tau) = \|U_\epsilon(x,t) - U^{(1,2)}(x,t;\rho^*,\tau)\|_{H^1} \tag{13}$$

To determine the closest element of $U^{(1,2)}(x,t;\rho^*,\tau)$ to the perturbed solution we let

$$\mathcal{H}^{(1,2)}_{\max}(\rho^*,\tau) = \max_{t\in[0,30]}\mathcal{H}^{(1,2)}(t;\rho^*,\tau) \tag{14}$$

and then determine the unique τ^* which minimizes $\mathcal{H}^{(1,2)}_{\max}(\rho^*,\tau)$, i.e

$$\mathcal{H}^{(1,2)}_{\mathrm{mm}} = \min_\tau \mathcal{H}^{(1,2)}_{\max}(\rho^*,\tau) = \mathcal{H}^{(1,2)}_{\max}(\rho^*,\tau^*). \tag{15}$$

As before, the ensemble measure of closeness, $\mathcal{A}_i^{(1,2)}(t)$, is the average of $\mathcal{H}^{(1,2)}(t;\rho^*,\tau^*)$ over all 100 simulations for each f_i.

Figure 7a and b show $\mathcal{H}^{(1,2)}_{\max}(\rho^*,\tau)$ for initial data (Eq. 9) with $f_i(x) = f_4(x)$ and $f_i(x) = f_5(x)$, respectively. In Fig. 7a $\mathcal{H}^{(1,2)}_{\mathrm{mm}} \sim 0.0091$ at $\tau^* \sim -10.44$ and in Fig. 7b $\mathcal{H}^{(1,2)}_{\mathrm{mm}} \sim 0.2068$ at $\tau^* \sim -10.06$. Figure 8 provides the contours of the perturbed solution for

NHESSD
1, 5087–5115, 2013

$f_i(x) = f_4(x)$ along with (a) $U^{(1,2)}(x,t;\rho^*,\tau_0)$ where the first mode has been matched using ρ^* and τ is kept at it's original value τ_0 and (b) $U^{(1,2)}(x,t;\rho^*,\tau^*)$, the nearest two-mode SPB found by minimizing $\mathcal{H}^{(1,2)}_{\max}(\rho^*,\tau)$. Similarly, Fig. 9 shows the contours when $f_i(x) = f_5(x)$. Here, the nearest two-mode SPB found by minimizing $\mathcal{H}^{(1,2)}_{\max}(\rho^*,\tau)$, produces a match only in time. The perturbation introduces spatial asymmetry that cannot be ameliorated by the matching procedure. Figure 10 provides the evolution of $\mathcal{A}^{(1,2)}_i(t)$. There is larger growth in $\mathcal{A}^{(1,2)}_i(t)$ than in $\mathcal{A}^{(1)}_i(t)$ for the one-mode SPB over a plane wave with UM since the spatial asymmetry has the opportunity to further develop with the second mode appearing at $t \approx 20$.

There is a larger variance in $\mathcal{H}^{(1,2)}_{\text{mm}}$; this can be seen in Table 1 where we provide the minimum, mean, median and maximum of $\mathcal{H}^{(1,2)}_{\text{mm}}$ over the entire ensemble of experiments for each f_i. We find $\mathcal{H}^{(1,2)}_{\text{mm}}$ is at most $\mathcal{O}(10^{-1})$ (obtained with the random phase f_1), with all other f_i yielding smaller asymmetries and f_6, the random high frequency perturbation, yielding the smallest. One may ask whether the observed spatial asymmetry can be captured explicitly by finding the solutions of Eq. (5) since, for random variations in the data, the squared eigenfunctions will no longer be centered about the origin. Since $\mathcal{A}^{(1,2)}_i(t)$ grows to at most $\mathcal{O}(10^{-1})$, $U_\epsilon(x,t)$ stays near to $U^{(1,2)}(x,t;\rho^*,\tau^*)$ for a substantial period of time, i.e. the two-mode SPB over a plane wave with two UMs is neutrally stable.

Figure 11 shows the special case of a perturbed coalesced two-mode SPB over a plane wave with two UMs (recall Fig. 2b). The ensemble closeness measurement $\mathcal{A}^{(1,2)}_i(t)$ is significantly smaller than in the generic two-mode SPB case (compare Figs. 11b and 10) and is on the order of $\mathcal{A}^{(1)}_i(t)$. In this case $U_\epsilon(x,t)$ stays nearer to $U^{(1,2)}(x,t;\rho^*,\tau^*)$ since the coalesced modes appear together earlier in time and as such $U_\epsilon(x,t)$ is not as susceptible to growth in spatial asymmetries. Surprisingly, the coalesced two-mode SPB appears to also be more robust under certain types of perturbations of the NLS equation (Calini and Schober, 2002). These two observations

NHESSD
1, 5087–5115, 2013

indicate that the coalesced case may be the most robust two-mode SPB in a laboratory setting.

4 Squared eigenfunctions and linear stability

To support the results of the numerical investigation this section provides an outline of our linear stability analysis of the one- and two-mode SPB solutions (see Calini and Schober, 2013). The key step in the analysis is to note that for a solution $u(x,t)$ of the NLS equation, e.g. one of the SPBs, its corresponding "squared eigenfunctions" satisfy the linearized equation about $u(x,t)$, i.e. Eq. (5) with $u_a(x,t)$ replaced by a general $u(x,t)$. In particular, for a one-mode SPB, if $\boldsymbol{\phi}$ and $\boldsymbol{\psi}$ satisfy the Z–S system (Eq. 2) for $U^{(j)}(x,t)$, then $f(x,t) = \phi_1\psi_1 + \bar{\phi}_2\bar{\psi}_2$ and $g(x,t) = \mathrm{i}(\phi_1\psi_1 - \bar{\phi}_2\bar{\psi}_2)$ solve Eq. (5). Thus, determining stability becomes simply a question of examining the behavior in time of $f(x,t)$ and $g(x,t)$.

The Bäcklund-gauge transformation (Sattinger and Zurkowski, 1987) allows one to transform both the base solution $u(x,t)$ and its eigenfunctions, while maintaining spatial periodicity, as follows: Let $\boldsymbol{\phi} := \alpha_+\boldsymbol{\phi}^+ + \alpha_-\boldsymbol{\phi}^-$, $\alpha_\pm \in \mathbb{C}$, where $\boldsymbol{\phi}^+$, $\boldsymbol{\phi}^-$ independently solve the Z–S system at (u,λ_j), where λ_j is one of the complex λ_j^{d}. The gauge matrix is given by

$$\mathbf{G}(\lambda;\lambda_j,\boldsymbol{\phi}) = \begin{pmatrix} \lambda - \lambda_j \frac{|\phi_1|^2-|\phi_2|^2}{|\phi_1|^2+|\phi_2|^2} & -\lambda_j \frac{2\phi_1\bar{\phi}_2}{|\phi_1|^2+|\phi_2|^2} \\ -\lambda_j \frac{2\bar{\phi}_1\phi_2}{|\phi_1|^2+|\phi_2|^2} & \lambda + \lambda_j \frac{|\phi_1|^2-|\phi_2|^2}{|\phi_1|^2+|\phi_2|^2} \end{pmatrix}.$$

Then

$$\boldsymbol{\phi}^{(j)}(x,t,\lambda;\lambda_j) = \mathbf{G}(\lambda;\lambda_j,\boldsymbol{\phi})\boldsymbol{\phi}(x,t,\lambda) \tag{16}$$

NHESSD
1, 5087–5115, 2013

solves the Z–S system (Eq. 2) at $(U^{(j)}(x,t),\lambda)$, where

$$U^{(j)}(x,t) = u + 2(\lambda_j - \bar{\lambda}_j)\frac{\phi_1\bar{\phi}_2}{|\phi_1|^2 + |\phi_2|^2} \tag{17}$$

is the new NLS solution. Notationally, the number of superscripts implies the number of times the transformatin has been applied, while the value of the superscript j indicates which λ_j is used in the transformation.

When the base solution is an unstable plane wave, for each complex λ_j^{d}, the new solution $U^{(j)}(x,t)$ is the one-mode SPB over the plane wave corresponding to the jth UM. Iterating the Bäcklund-gauge transformation provides a two-mode SPB, for example, $U^{(1,2)}(x,t)$ and it's corresponding eigenfunctions. Since we are interested in the stability of the SPBs so we focus only on the form of the transformed eigenfunctions. The independent eigenfunctions corresponding to the plane wave are, for $k(\lambda) = \sqrt{\lambda^2 + a^2}$,

$$\boldsymbol{\phi}^{\pm}(x,t;\lambda) = \frac{\mathrm{e}^{\mp \mathrm{i}\pi/4}}{2k(\lambda)} \begin{pmatrix} \sqrt{a\,(k(\lambda)\pm\lambda)}\mathrm{e}^{\mathrm{i}a^2 t} \\ \pm\sqrt{a(k(\lambda)\mp\lambda)}\mathrm{e}^{-\mathrm{i}a^2 t} \end{pmatrix} \times \mathrm{e}^{\pm\mathrm{i}(k(\lambda)x + 2\lambda k(\lambda)t)}.$$

If the plane wave has only one UM corresponding to complex λ_1^{d}, the elements of $\mathbf{G}(\lambda;\lambda_j,\boldsymbol{\phi})$ are bounded in time since

$$\frac{|\phi_1|^2 - |\phi_2|^2}{|\phi_1|^2 + |\phi_2|^2} = \frac{\cos p \sin(2kx+\beta)}{\cosh(\rho - \sigma t) + \sin p \cos(2kx+\beta)},$$

$$\frac{2\phi_1\bar{\phi}_2}{|\phi_1|^2 + |\phi_2|^2} = a\mathrm{e}^{\mathrm{i}a^2 t} \times [\cos p \sinh(\rho - \sigma t) + \mathrm{i}\sin p \cosh(\rho - \sigma t)$$

NHESSD
1, 5087–5115, 2013

$$+ i\cos(2kx+\beta)]$$
$$\times[\cosh(\rho-\sigma t)+\sin p\cos(2kx+\beta)]^{-1}, \quad (18)$$

where $\mu_1 = 2k(\lambda_1) = 2\pi/L$. From these expressions we see the only possible source of exponential growth from $f(x,t)$ and $g(x,t)$ are those formed using the following eigenfunctions

$$\boldsymbol{\chi}^{\pm}(x,t;\lambda_1) = \mathbf{G}(\lambda;\lambda_1,\boldsymbol{\phi})\boldsymbol{\phi}^{\pm}(x,t;\lambda)|_{\lambda=\lambda_1}.$$

It is sufficient to examine the behavior of $\boldsymbol{\chi}^{+}$ since $\boldsymbol{\chi}^{\pm}$ are linearly dependent at $\lambda=\lambda_1$. We find $\boldsymbol{\chi}^{+}(x,t;\lambda_1)$ does not grow exponentially as

$$\boldsymbol{\chi}^{+}(x,t;\lambda_1) \sim \begin{pmatrix} \frac{\bar{\phi}_2}{|\phi_1|^2+|\phi_2|^2} \\ \frac{-\phi_1}{|\phi_1|^2+|\phi_2|^2} \end{pmatrix},$$

with

$$\frac{\phi_1}{|\phi_1|^2+|\phi_2|^2} \sim \left[e^{i\left(\frac{\pi}{L}x+\frac{\beta}{2}+\frac{p}{2}\right)}e^{-(\sigma t-\rho)/2} + i\,e^{-i\left(\frac{\pi}{L}x+\frac{\beta}{2}+\frac{p}{2}\right)}e^{(\sigma t-\rho)/2}\right] \times\left[\cosh(\rho-\sigma t)+\sin p\cos\left(\frac{2\pi}{L}x+\beta\right)\right]^{-1},$$

Likewise, the first component is also bounded in time. Thus the solutions to the linearized equation, $f(x,t)$ and $g(x,t)$, are bounded in time. As a result we find the Bäcklund transformation at λ_1 saturates the corresponding UM of the plane wave and the one-mode SPB is neutrally stable when the underlying plane wave has only one UM.

Similarly, if the plane wave has only two unstable modes then iterating the Bäcklund transformations at the associated spectral elements λ_1 and λ_2 will saturate the linear

NHESSD
1, 5087–5115, 2013

instabilities of the corresponding UMS of the plane wave. Thus the two-mode SPBs over a plane wave with two UMS, $U^{(1,2)}(x,t;\rho,\tau)$, are neutrally stable.

However, a one-mode SPB over the plane wave with 2 unstable modes can be shown to be linearly unstable. In this case, if $U^{(1)}(x,t;\rho)$ is produced by applying transformation (Eq. 17) at λ_1 then the two corresponding eigenfuctions $\boldsymbol{\chi}^{\pm}(x,t;\lambda)$ are linearly independent at $\lambda=\lambda_2$ and exhibit exponential growth in time, i.e., the first component is of the form

$$\chi_1^{\pm}(x,t;\lambda_2) \sim \exp\left(\pm\frac{\sigma t}{2}\right)\cdot B_{\pm}(x,t),$$

where $B_{\pm}(x,t)$ are bounded and σ is real, $\sigma=-4\mathrm{i}\lambda_2 k(\lambda_2)$. In this case $f(x,t)$ and $g(x,t)$ grow exponentially fast and $U^{(1)}(x,t;\rho)$ is linearly unstable. These results indicate that only those SPBs for which all the instabilities of the underlying plane wave are saturated are neutrally stable.

Acknowledgements. The authors gratefully acknowledge the support of the National Science Foundation through grants DMS-1109017 and DMS-1108973.

References

Akhmediev, N., Ankiewicz, A., and Taki, M.: Waves that appear from nowhere and disappear without a trace, Phys. Lett. A, 373, 675–678, 2009a. 5089

Akhmediev, N., Soto-Crespo, J. M., and Ankiewicz, A.: Extreme waves that appear from nowhere: on the nature of rogue waves, Phys. Lett. A, 373, 2137–2145, 2009b. 5089

Ankiewicz, A., Clarkson, P. A., and Akhmediev, N.: Rogue waves, rational solutions, the patterns of their zeros and integrable relations, J. Phys., 43, 1–9, 2010. 5089

Calini, A. and Schober, C. M.: Homoclinic chaos increases the likelihood of rogue waves, Phys. Lett. A, 298, 335–349, 2002. 5089, 5090, 5093, 5098

Calini, A. and Schober, C. M.: Rogue waves in higher order nonlinear Schrödinger models, in: Extreme Ocean Waves, 31–51, edited by: Pelinovsky, E. and Kharif, C., Springer, 2009. 5090

NHESSD

1, 5087–5115, 2013

Calini, A. and Schober, C. M.: Observable and reproducible rogue waves, J. Optics, 15, doi:10.1088/2040-8978/15/10/105201, 2013. 5099

Dysthe, K. and Trulsen, K.: Note on breather type solutions of the NLS as model for freak waves, Phys. Scripta, T82, 48–52, 1999. 5089

Khaliq, A. Q. M., Martin-Vaquero, J., Wada, B. A., and Yousuf, M.: Smoothing schemes for reaction-diffusion systems with nonsmooth data, J. Comput. Appl. Math., 223, 374–386, 2009. 5093

Ohta, Y. and Yang, J.: General high-order rogue waves and their dynamics in the nonlinear Schrödinger equation, P. R. Soc. A, 468, 1716–1740, 2012. 5089

Osborne, A., Onorato, M., and Serio, M.: The nonlinear dynamics of rogue waves and holes in deep-water gravity wave trains, Phys. Lett. A, 275, 386–393, 2000. 5089

Sattinger, D. H. and Zurkowski, V. D.: Gauge theory of Bäcklund transformations, Physica D, 26, 225–250, 1987. 5099

Zakharov, V. E. and Shabat, A. B.: Exact theory of two-dimensional self-focusing and one-dimensional self-modulation of waves in nonlinear media, J. Exp. Theor. Phys., 34, 62–69, 1972. 5090

NHESSD

1, 5087–5115, 2013

Numerical study of stability of breathers

A. Calini and C. M. Schober

Table 1. The minimum, mean, median and maximum of $\mathcal{H}_{\mathrm{mm}}^{(1,2)}$ obtained in the ensemble of 100 experiments for each f_i.

f_i	Minimum	Mean	Median	Maximum
f_1	1.7616×10^{-7}	6.5183×10^{-3}	2.9831×10^{-5}	2.1138×10^{-1}
f_2	6.2504×10^{-7}	2.2224×10^{-3}	1.2596×10^{-5}	1.1811×10^{-1}
f_3	1.3286×10^{-6}	3.5547×10^{-3}	3.1829×10^{-5}	2.6490×10^{-1}
f_4	2.1195×10^{-7}	1.2651×10^{-3}	1.2519×10^{-5}	7.4857×10^{-2}
f_5	2.8895×10^{-7}	6.1313×10^{-4}	7.2525×10^{-6}	2.9186×10^{-2}
f_6	2.9967×10^{-7}	4.2785×10^{-4}	2.8146×10^{-6}	2.8567×10^{-2}

NHESSD
1, 5087–5115, 2013

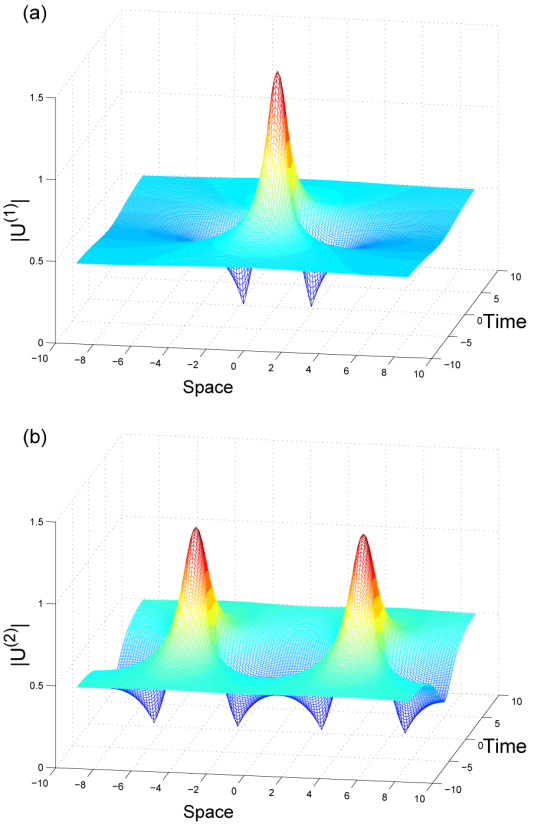

Fig. 1. Amplitude of a one-mode SPB over an unstable plane wave with two UMs: **(a)** $U^{(1)}(x,t;\rho)$ and **(b)** $U^{(2)}(x,t;\rho)$.

NHESSD
1, 5087–5115, 2013

Numerical study of stability of breathers

A. Calini and
C. M. Schober

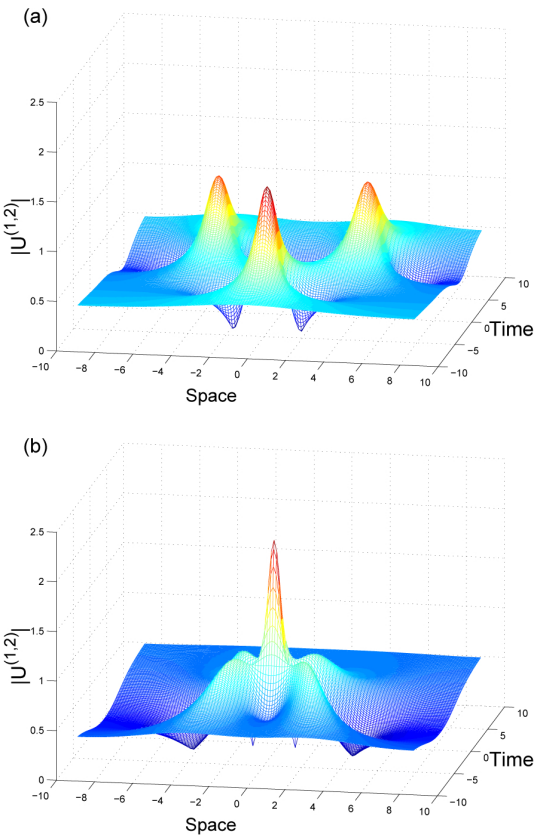

Fig. 2. Amplitude plots of the two-mode SPB over a plane wave with two UMs when the modes are **(a)** distinct and **(b)** coalesced.

NHESSD
1, 5087–5115, 2013

Numerical study of stability of breathers

A. Calini and
C. M. Schober

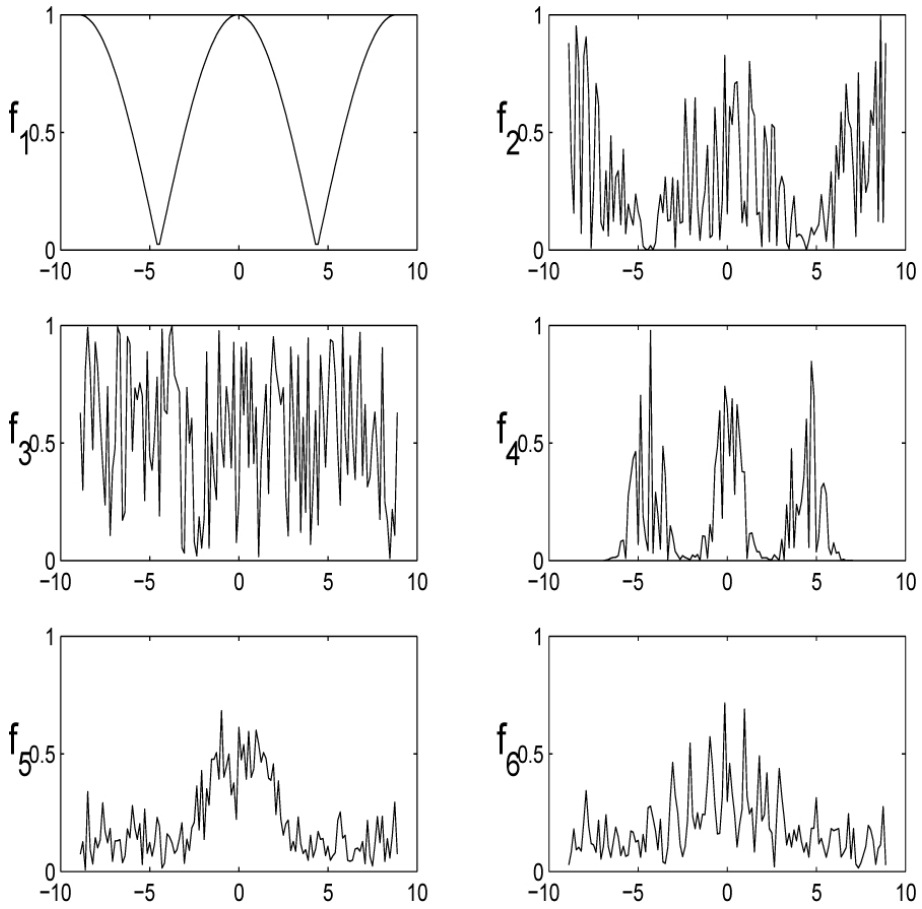

Fig. 3. Initial periodic perturbations f_i, $i = 1, \ldots, 6$.

NHESSD
1, 5087–5115, 2013

Numerical study of stability of breathers

A. Calini and
C. M. Schober

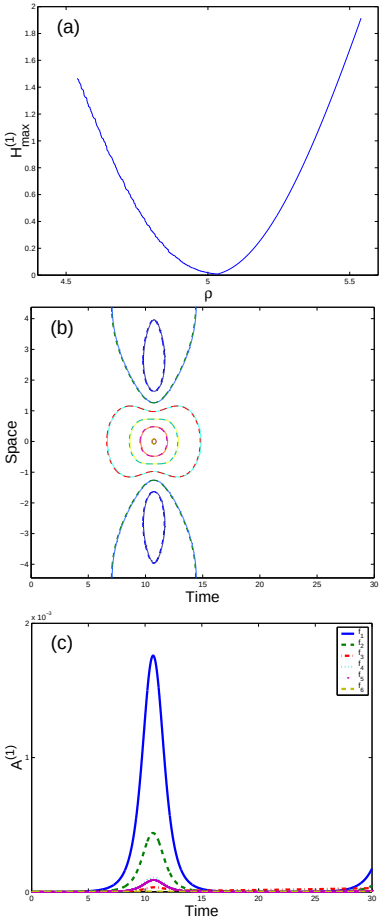

Fig. 4. (a) $\mathcal{H}^{(1)}_{\max}(\rho)$ **(b)** contours of $|U_\epsilon(x,t)|$ (dashed line) and the one-mode SPB $|U^{(1)}(x,t;\rho^*)|$ (solid line) over **(a)** plane wave with one UM. **(c)** Evolution of $\mathcal{A}^{(1)}_i(t)$ for each f_i.

NHESSD
1, 5087–5115, 2013

Numerical study of stability of breathers

A. Calini and
C. M. Schober

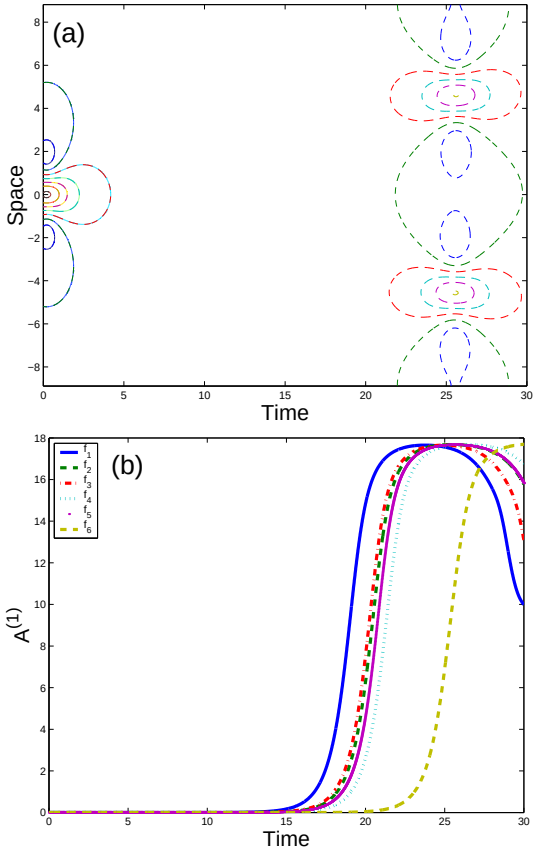

Fig. 5. (a) Contours of $|U_e(x,t)|$ (dashed line) and the one-mode SPB $|U^{(1)}(x,t;\rho^*)|$ (solid line) over a plane wave with two UMs. **(b)** Evolution of $\mathcal{A}_i^{(1)}(t)$ for each f_i.

NHESSD
1, 5087–5115, 2013

Numerical study of stability of breathers

A. Calini and
C. M. Schober

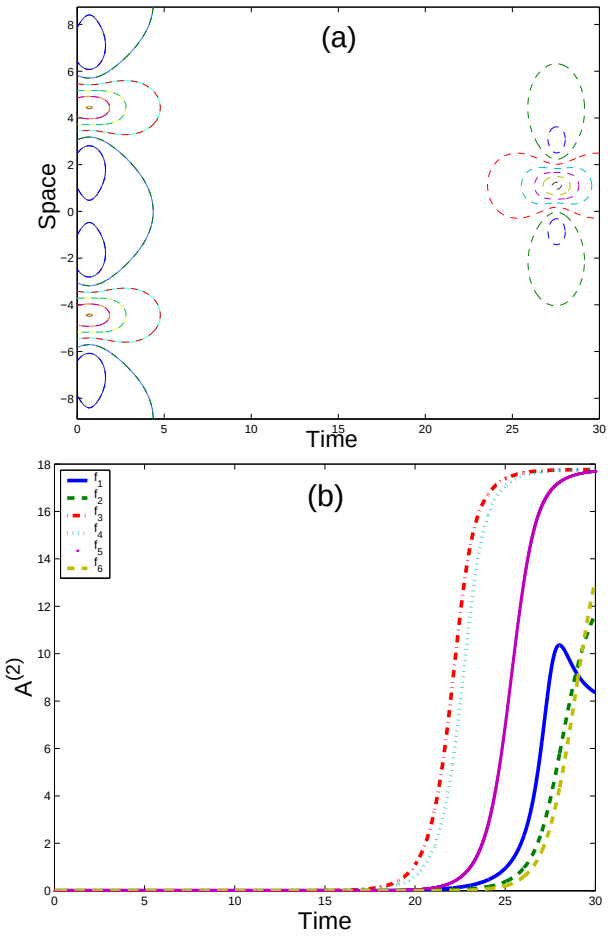

Fig. 6. (a) Contours of $|U_e(x,t)|$ (dashed line) and the one-mode SPB $|U^{(2)}(x,t;\rho^*)|$ (solid line) over a plane wave with two UMs. **(b)** Evolution of $\mathcal{A}_i^{(2)}(t)$ for each f_i.

NHESSD
1, 5087–5115, 2013

Numerical study of stability of breathers

A. Calini and
C. M. Schober

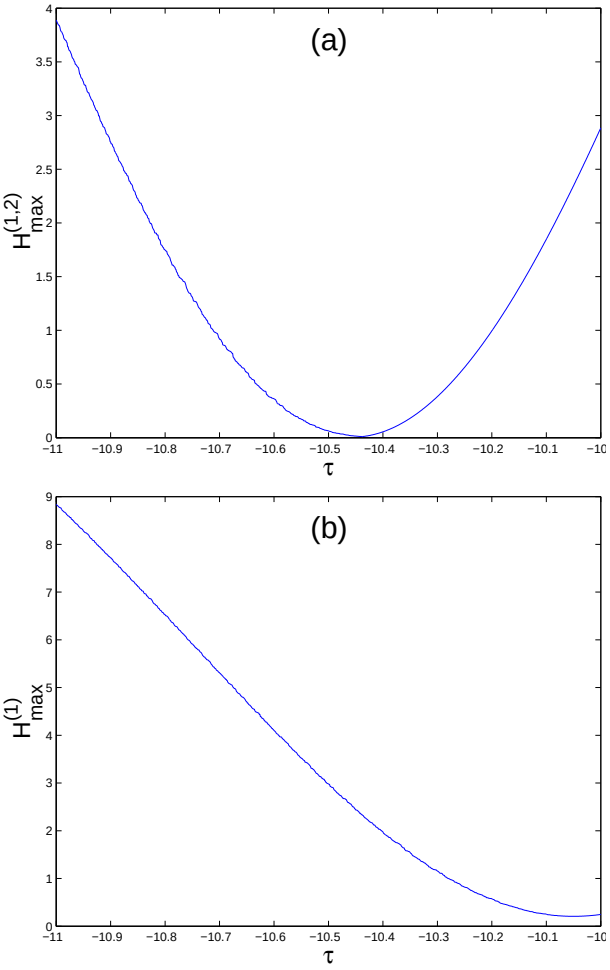

Fig. 7. $\mathcal{H}^{(1,2)}_{\max}(\rho^*, \tau)$ for **(a)** $f_4(x)$ and **(b)** $f_5(x)$. $\mathcal{H}^{(1,2)}_{\mathrm{mm}}$ is ~ 0.0091 and ~ 0.2068, respectively.

NHESSD
1, 5087–5115, 2013

Numerical study of stability of breathers

A. Calini and
C. M. Schober

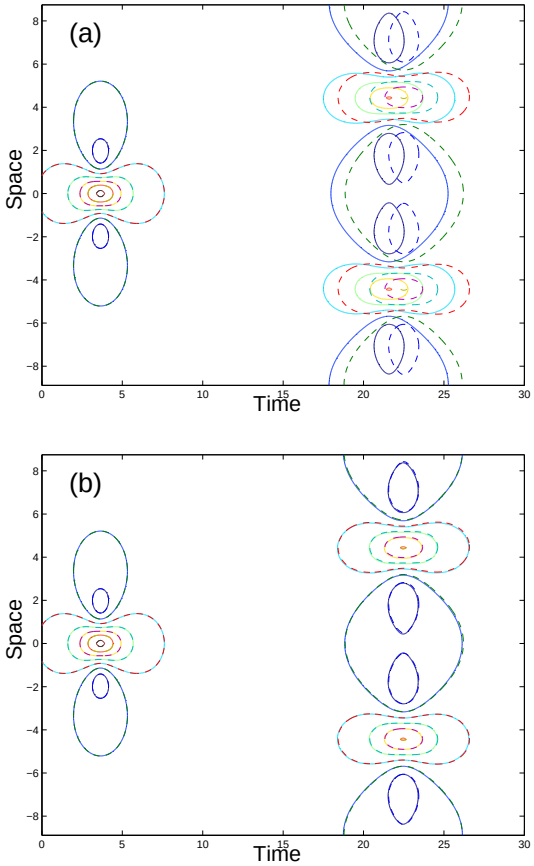

Fig. 8. (a) Contours of $|U_\epsilon(x,t)|$ for $f_4(x)$ (dashed line) and the two-mode SPB (solid line) given by **(a)** $|U^{(1,2)}(x,t;\rho^*,\tau_0)|$, and **(b)** $|U^{(1,2)}(x,t;\rho^*,\tau^*)|$.

NHESSD
1, 5087–5115, 2013

Numerical study of stability of breathers

A. Calini and
C. M. Schober

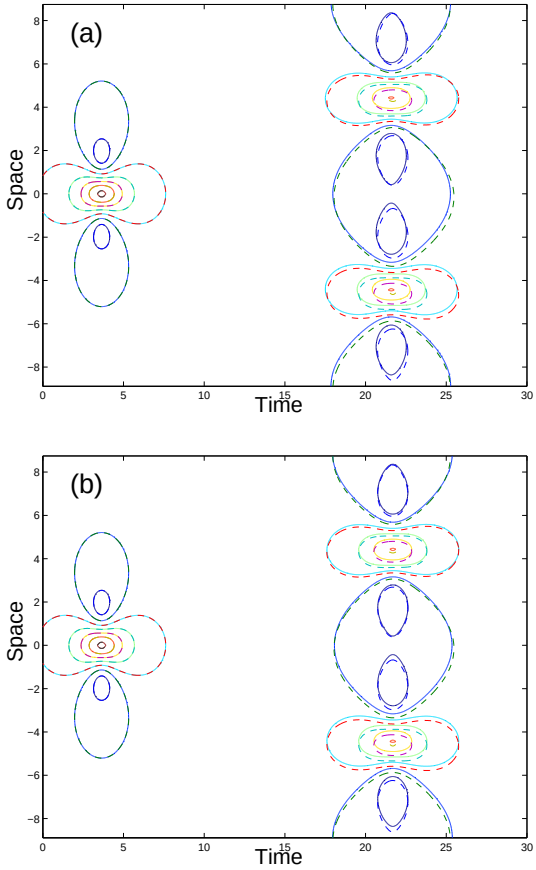

Fig. 9. Contours of $|U_e(x,t)|$ for $f_5(x)$ (dashed line) and the two-mode SPB (solid line) given by **(a)** $|U^{(1,2)}(x,t;\rho^*,\tau_0)|$, and **(b)** $|U^{(1,2)}(x,t;\rho^*,\tau^*)|$.

NHESSD
1, 5087–5115, 2013

Numerical study of stability of breathers

A. Calini and
C. M. Schober

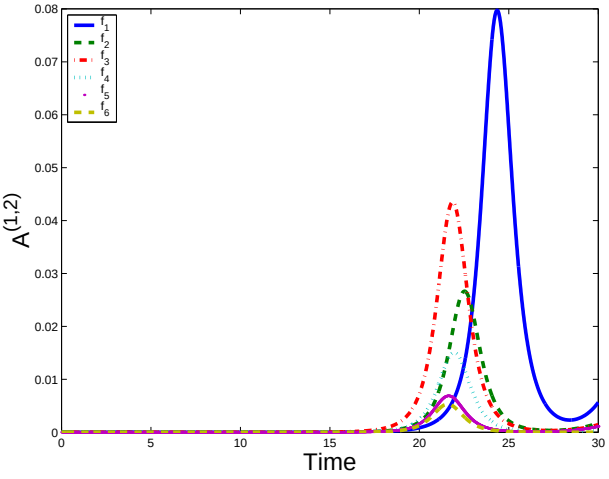

Fig. 10. Evolution of $\mathcal{A}_i^{(1,2)}(t)$ for each f_i.

NHESSD
1, 5087–5115, 2013

Numerical study of stability of breathers

A. Calini and
C. M. Schober

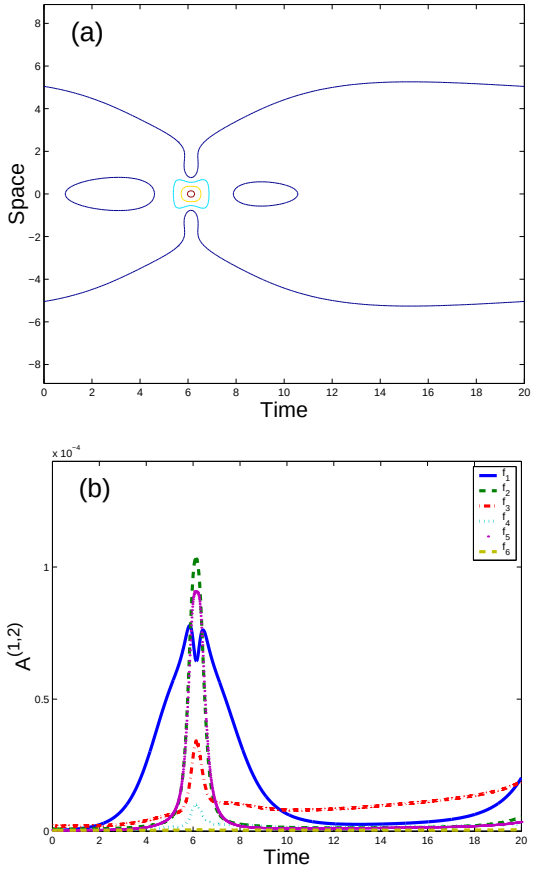

Fig. 11. (a) Contours of $|U_\epsilon(x,t)|$ in the coalesced case for $f_5(x)$ (dashed line) and of the two-mode SPB $|U^{(1,2)}(x,t;\rho^*,\tau^*)|$ (solid line) given by **(a)** $|U^{(1,2)}(x,t;\rho^*,\tau^*)|$, and **(b)** evolution of $\mathcal{A}_i^{(2)}(t)$ for each f_i.

NHESSD
1, 5087–5115, 2013

Numerical study of stability of breathers

A. Calini and
C. M. Schober